Individual microtubule dynamics contribute to the function of mitotic and cytoplasmic arrays in fission yeast

Meredith Johnson Sagolla, Satoru Uzawa and W. Zacheus Cande*

Department of Molecular and Cell Biology and Department of Plant and Microbial Biology, University of California Berkeley, Berkeley, CA 94720-3200, USA

*Author for correspondence (e-mail: zcande@uclink4.berkeley.edu)

Accepted 24 July 2003
Journal of Cell Science 116, 4891-4903 © 2003 The Company of Biologists Ltd
doi:10.1242/jcs.00796

Summary

Schizosaccharomyces pombe **is an excellent organism for studying microtubule dynamics owing to the presence of well-defined microtubule arrays that undergo dramatic rearrangements during various stages of the cell cycle. Using sensitive time-lapse video microscopy and kymographic analysis, we have determined the polymerization/depolymerization kinetics of individual microtubules within these arrays throughout the fission yeast cell cycle. Interphase bundles are composed of 4-7 microtubules that act autonomously, demonstrating that individual microtubules are responsible for mediating the functions ascribed to these arrays. The nucleation and growth of cytoplasmic microtubules is inhibited upon cellular transition into mitosis, leading to their gradual disappearance. At the onset of mitosis, microtubules form on the nuclear face of the spindle pole body and exhibit dramatically increased dynamics. The presence of these intra-nuclear astral microtubules (INA) is reminiscent of spindle assembly and the search and chromosome capture mechanism observed in metazoan cells. Consistent with other in vivo studies, we do not observe microtubule flux in the anaphase B spindle. Finally, the depolymerization of individual microtubules alternates between each half-spindle, resulting in spindle collapse during telophase. On the basis of these observations, we conclude that microtubules in these diverse cytoskeletal arrays have autonomous behaviors that are an essential component of any model describing cell-cycle-dependent changes in the behavior and function of microtubule arrays.**

Movies available online

Key words: Microtubule, Dynamics, Fission yeast, Mitosis, Spindle

Introduction

Eukaryotic cells depend on the microtubule cytoskeleton to carry out vital cellular processes. Microtubules have a wide range of functions at different cell-cycle stages that include maintenance of cell polarity and ensuring accurate chromosome segregation. Dynamic instability is an inherent property of microtubules. However, microtubule-associated proteins (MAPs) help to modulate microtubule dynamics during different stages of the cell cycle. Consistent with this, isolated bovine brain tubulin assembles into microtubule polymers at a much slower rate in vitro than is seen in vivo (Horio and Hotani, 1986), a difference that is attributed to the function of MAPs in vivo. Cell-cycle-dependent MAP function may help to explain the dramatic change in the half-life of microtubules that occurs between interphase and mitosis in metazoan cells. At this transition, the microtubule half-life decreases tenfold as the cells enter mitosis (Hayden et al., 1990; Inoue and Salmon, 1995). This change in microtubule dynamics is thought to facilitate formation of the bipolar spindle and attachment of chromosomes to kinetochore microtubules (Hayden et al., 1990). Given our prior knowledge of microtubule behavior, an important question remains unaddressed: how does the behavior of individual microtubules contribute to the function of larger microtubule arrays?

The fission yeast *Schizosaccharomyces pombe* is an excellent organism for the study of microtubule dynamics. In these cells, well-defined microtubule arrays undergo dramatic rearrangements at various points in the cell cycle. During interphase, the microtubules are organized into discrete bundles that extend from the nucleus to the cell tips (Fig. 1A). Microtubules in the bundle overlap at the cell center in an antiparallel orientation with the plus ends near the cell tips (Tran et al., 2001). The number of bundles varies throughout interphase from as few as one to as many as eight (Hagan and Hyams, 1988). The highly organized nature of fission yeast interphase microtubules allows for easy visualization and characterization of individual microtubules within these arrays. Microtubule arrays are reorganized at distinct stages of the cell cycle, with each new array possessing a specific function in different cellular processes. These functions can be described either by the collective or individual activities of the microtubules that comprise the arrays.

At the transition to mitosis, cytoplasmic arrays disappear and are replaced by an intra-nuclear spindle, marking a dramatic change in microtubule organization and dynamic properties in *S. pombe* cells (Fig. 1A). The spindle consists of 12-14 polar microtubules nucleated from each spindle pole

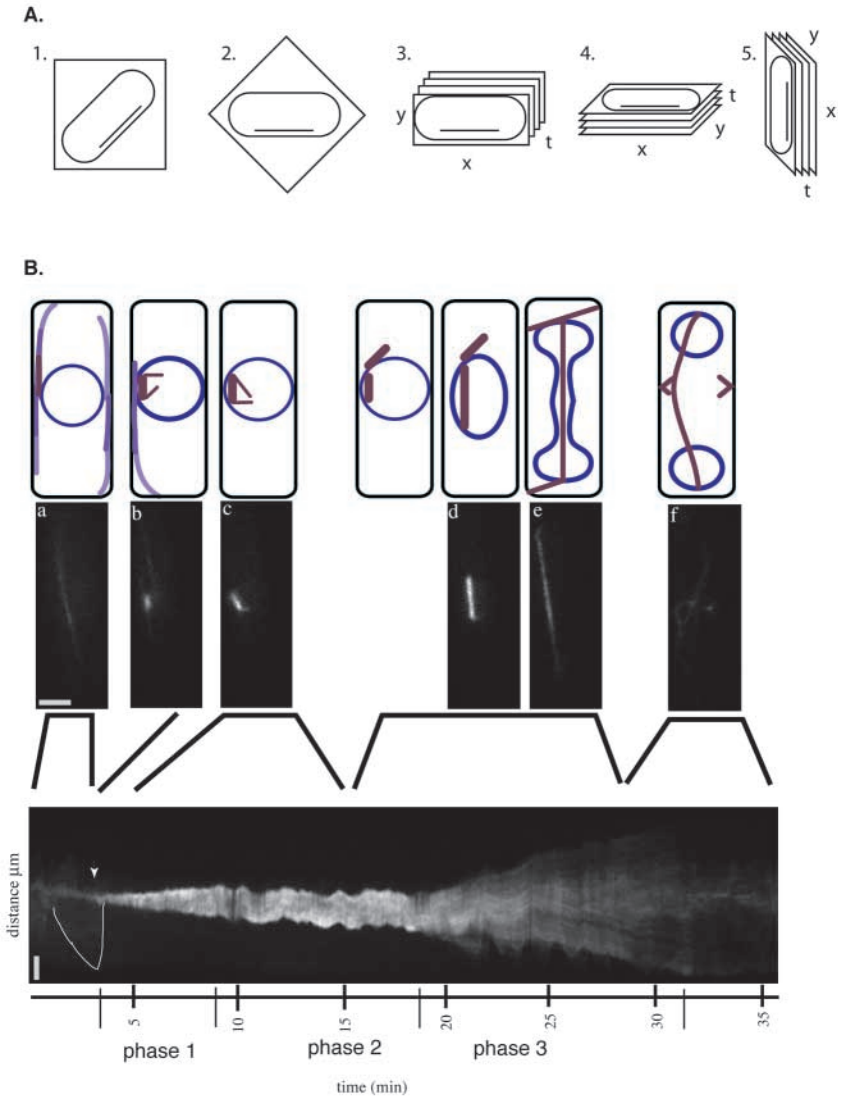

Fig. 1. Microtubule arrays in the fission yeast cell cycle are depicted by cartoon, still images and kymograph. (A) Description of how to construct a kymograph from a series of time-lapse images using DeltaVision software: 1. A series of time-lapse images were taken of a cell of interest. 2. The images were rotated to orient the microtubule of interest along the horizontal axis. 3. The images were then cropped around the cell boundary and the time-lapse images were converted into a 3D stack. 4. The stack of images were rotated 90° around the horizontal axis to align the time points in a vertical stack; this allows for the changes in microtubule length overtime to be seen as a line trace or kymograph. 5. The kymograph was then rotated so that time is on the horizontal axis. (B) The top panel shows a schematic demonstrating the different microtubule arrays as they appear in various stages of the cell cycle. The middle panel shows still images of a cell expressing GFP:α-tubulin (YY105) taken from a time-lapse movie of a cell progressing from G2 through telophase. Images correspond to the cartoon drawings and to the areas marked on the kymograph (lower panel): (a) G2-interphase, (b) G2-M transition with stage 1 spindle, (c) phase 2 spindle, (d) early anaphase B, (e) late anaphase B, and (f) telophase. Bar, 2 μm. The lower panel shows a kymograph made from the same time-lapse movie as the images shown in the middle panel. The images a-f in the middle panel correspond to the indicated regions of the kymograph. The kymograph is presented with time in minutes progressing along the horizontal axis and the length of the cell on the vertical axis. The three spindle phases are labeled below the kymograph. The transition from G2-M is marked with an arrow. The white outline marks triangular area of fluorescence that marks the life history of an interphase half bundle. Bar, 2 μm.

body (SPB) and 3-4 kinetochore microtubules per chromosome (Ding et al., 1993). Photobleaching experiments have demonstrated that the turnover of tubulin is more rapid in metaphase than in anaphase, demonstrating that there is a change in microtubule properties between these two stages (Mallavarapu et al., 1999). Earlier stages of spindle formation have not been carefully analyzed.

The final mitotic microtubule arrays that form appear in late anaphase, when equatorial microtubule-organizing centers (MTOCs) are activated in the cell center, and demarcate the future site of cytokinesis (Hagan, 1998; Hagan and Hyams, 1988; Hagan and Petersen, 2000; Heitz et al., 2001). From these central MTOCs, new cytoplasmic microtubule arrays form both an equatorial ring and two prominent small asters at the cell midzone. Microtubules extending from the small asters reconstitute the interphase arrays for the newly formed daughter cells.

To gain a better understanding of the cell-cycle-dependent role of microtubule arrays in *S. pombe*, a more fundamental understanding of the behavior of individual microtubules that comprise the arrays is necessary. We have employed high-speed video microscopy coupled with kymographic analysis to visualize and quantify the movements of individual microtubules throughout the cell cycle. This approach enabled the movements of single microtubules within the arrays to be followed, and the rates of microtubule polymerization and depolymerization to be measured. Our observations provide important new insights into the details of individual microtubule behavior in interphase and mitotic arrays. How properties of individual microtubules affect the functions of more complex arrays is discussed.

Materials and Methods

Yeast strains

The strains used in this analysis include: YY105 (h90 leu1-32 ura4-D18 lys1+:: [GFP:atb2]) and YY106 (h90 leu1-32 ura4-D18 lys1+:: [GFP:atb2]/pD817). Plasmid pD817 contains GFP:cytochrome P450 reductase, ars1, LEU2 (Tange et al., 1998). These strains and plasmids were the kind gifts of Da Qiao Ding and Yasushi Hiraoka (Kamsai Advanced Research Center, Kobe, Japan). Also used in certain experiments was strain 2694 (h^{-} $leu1^{-}$ ade6-210 ura4-D18 GFP:Swi6 GFP:atb2), which was a gift from Alison Pidoux (Pidoux et al., 2000). Cells were grown on rich YES or minimal selective media plates at either 25°C or 30°C (Egel et al., 1994; Moreno et al., 1991).

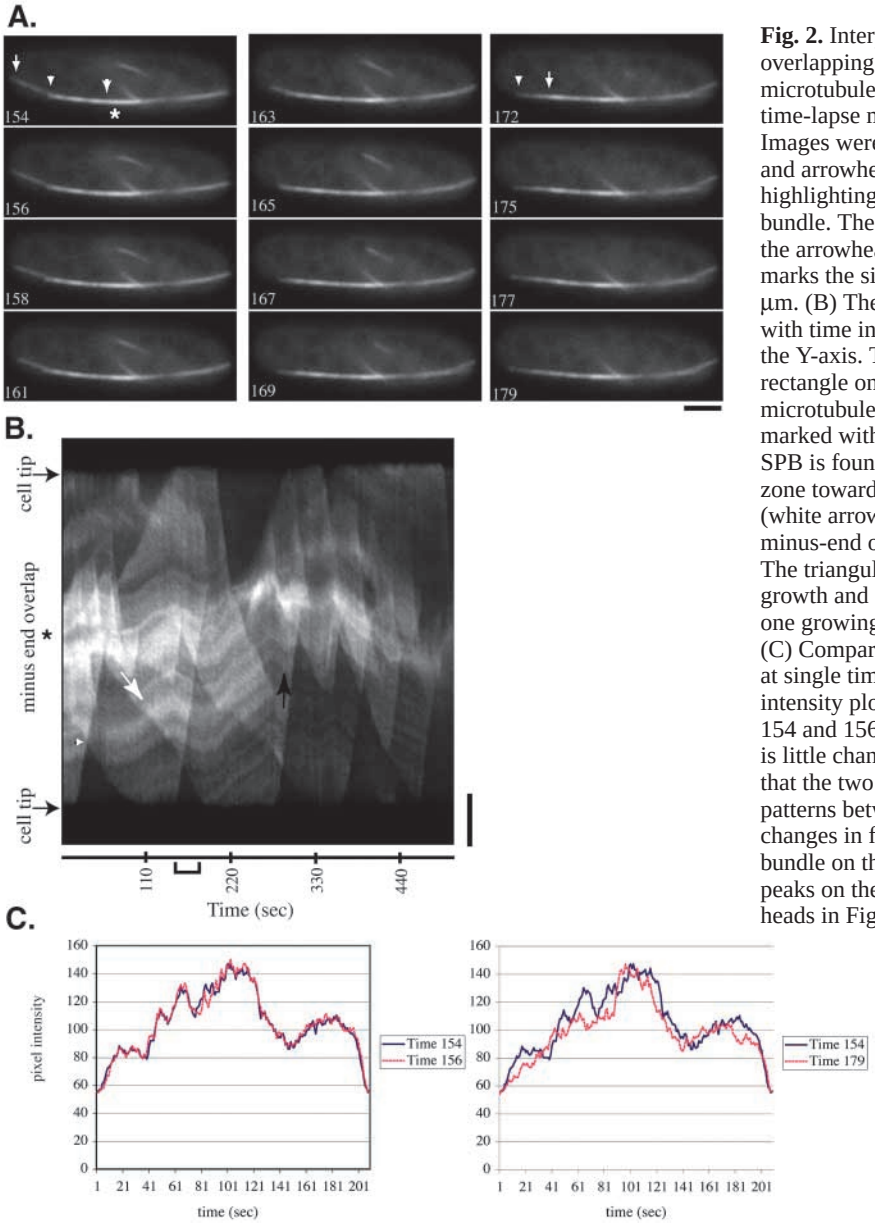

Fig. 2. Interphase microtubule arrays are composed of overlapping half bundles of 2-3 autonomously behaving microtubules. (A) Shown here are sequential images from a time-lapse movie of a cell expressing GFP:α-tubulin (YY105). Images were taken at approximately 2-second intervals. Arrows and arrowheads mark the plus ends of individual microtubules, highlighting the presence of multiple microtubules in each bundle. The arrow points to a microtubule that is shrinking and the arrowheads to microtubules that are growing. The asterisk marks the site where antiparallel microtubules overlap. Bar, 2 μm. (B) The same time-lapse movie presented as a kymograph with time in seconds along the X-axis and length of cell along the Y-axis. The time points shown in A are delineated with a rectangle on the time line of the kymograph. The region of the microtubule overlap that corresponds to the still images is marked with an asterisk; this also marks the region where the SPB is found. The lines descending from the minus-end overlap zone towards the cell tip reflect growth of a single microtubule (white arrow). Lines ascending from the cell tip toward the minus-end overlap zone reflect depolymerization (black arrow). The triangular regions of increased fluorescence intensity where growth and shrinkage lines intersect is due to the presence of one growing and one shrinking microtubule. Bar, 2 μm. (C) Comparison of pixel intensity along the microtubule bundle at single time points. The graph on the left compares the pixel intensity plots of two consecutive time points (seen in Fig. 2A), 154 and 156. The plots are almost identical, showing that there is little change in the composition of the microtubule bundle and that the two intensity plots show similar but not identical patterns between the two time points. The plots show five major changes in fluorescence intensity across the bundle. The half bundle on the left (Fig. 2A, time 154) shows three intensity peaks on the graph, which are marked by arrows and arrow heads in Fig. 2A (time 154). The overlap zone shows the area of greatest intensity. The half bundle on the right in Fig. 2A (time 154) shows a more dramatic decrease in intensity from the overlap zone and a pixel intensity of two microtubules. This is also evident in the graph shown here. The graph on the right compares time 154 with time 179, showing there were major changes in the intensity distribution and therefore the number of microtubules along the length of the bundle over time (see Movie 1, http://jcs.biologists.org/supplemental/).

Microscopy of living cells

For microscopy, cells were grown on rich YES or MSA minimal media plates (Egel et al., 1994; Moreno et al., 1991), and a small amount was scraped off plates and resuspended in 20 μl dH_2O or 5 μM n-propyl gallate to prevent photobleaching. 1-2 μl of this cell suspension was placed onto an agarose pad (1.1% Apex agarose in PM media) and sealed under a glass coverslip with silicone lubricant vacuum grease (Dow-Corning). Images were taken using an Olympus IX70 wide-field inverted fluorescence microscope with an Olympus UPlanApo 100×, NA 1.35, oil immersion objective. DeltaVision image acquisition software (Applied Precision, Issaquah, WA) was used to capture and process images obtained with a Photometrics CCD CH350 camera cooled to –35°C (Roper Scientific, Tuscon, AZ).

To observe microtubule bundles over time, we took sequential 0.3 second exposures of a single focal plane at an average of 2.0 seconds, which is the maximum acquisition speed of our system. The kymograph in Fig. 2 was made from a time-lapse movie in which we recorded 3 focal planes at 0.4 μm steps at 7-second intervals to capture microtubules in all focal planes. No deconvolution was used.

Kymograph reconstruction

The kymograph displays of mitotic spindles were constructed from a series of time-lapse movie images using the DeltaVision software. This technique is similar to that used by Maddox et al. (Maddox et al., 2000), and is depicted in Fig. 1A. The specifics of our method are explained as follows. The images were first rotated to align the selected microtubules along the horizontal axis. The images were then rotated 90.0° around the horizontal axis in order to display the time points as a stack of sequential images. Each time point represents one pixel line. Finally, the image was compressed into a 2D projection using the DeltaVision maximum intensity algorithm. Kymographs in the figures throughout this paper were rotated so that increasing time points would follow the horizontal axis from left to right.

Pixel intensity plots, seen in Fig. 2C, were made using the line profile function of the DeltaVision software package. Intensity values for all pixels in the kymograph were recorded as a text file and imported into Microsoft Excel for processing. The line values correspond to select time points shown in Fig. 2A. In order to determine the average pixel intensity for a single microtubule, first the

average background fluorescence intensity was determined [66.1 arbitrary units (a.u.)], and was then subtracted from the average pixel intensities calculated for each region of fluorescence we were interested in. The resulting graph shows four peaks with an interval of approximately 20 intensity values, which corresponds to the intensity of a single microtubule (average intensity of one microtubule is 84.1–66.1=18 a.u.). It was necessary to calculate the average pixel intensity for a region along the microtubule owing to the uneven incorporation of GFP:α-tubulin.

Measurements of INA microtubule activity

Our criteria for distinguishing INA microtubules were as follows: a bundle was counted if it was distinguishable from the spindle as a discrete oblique or perpendicular line. Consideration was not given to out-of-focus light unless a discrete microtubule was present in both adjacent frames (i.e. one before and one after). The duration of microtubule bundles was given the same consideration. The lifespan of a given bundle was determined by the total duration of time that the particular bundle appeared in the time-lapse movie. However, if a bundle disappeared but then reappeared in the same space in the following time frame, it was assumed that it went out of focus for one frame. To measure microtubule length, we used the 'Measure' feature of the DeltaVision software to determine the distance between the spindle pole and the tip of the INA microtubule. An average of three measurements was used on each individual bundle to avoid measurement errors. Ten individual INA microtubules were counted in two independent movies.

Measurement of microtubule growth/shrinkage

The rate of growth and shrinkage of individual microtubules was determined from the slope of a growing and shrinking microtubule in the kymographs. Rates were determined by measuring the ΔX (distance) and ΔY (time) in pixels for each line. In order to avoid inaccuracies of measuring an artificially straightened microtubule region, only regions of the microtubules that were straight in the time-lapse movie were used for measuring rates of growth and shrinkage. Each value for X and Y is the average of five separate time and distance measurements of four different microtubules. Each measurement was also corrected for oscillation of the midzone. ΔY was converted to seconds using the following equation: (ΔYpixels)×(2.2sec/pixel)=seconds. ΔX was converted to distance using the following equation: (ΔXpixels)/(15pixels/μm)=μm. Rate (μm/minute)=(length μm/seconds to disappear)×(60 seconds/1 minute).

Results

Rapid frame acquisition and kymographic analysis increase resolution of microtubule arrays

To examine the range of cell-cycle-dependent changes in microtubule behavior, we created time-lapse movies of cells expressing GFP:α-tubulin and displayed them as kymographs (Fig. 1B, lower panel). The consecutive frames of a time-lapse movie are represented in a kymograph in a single stack aligned along the X-axis. Kymographic analysis highlights cell-cycle-dependent changes in microtubule arrays as well as enabling the visualization of individual microtubules in these arrays. The methods used to create and display kymographs are shown in Fig. 1A. For example, in interphase, the combined growth and shrinkage of microtubules creates a triangular fluorescent region, which describes the life history of that particular microtubule. The triangle edge is outlined in Fig. 1B, lower panel.

At the transition to mitosis, the interphase arrays dwindle as the spindle begins to form in the nucleus (arrow Fig. 1B, lower panel). Additionally, the three distinct phases of growth for the mitotic spindle previously reported are evident in the kymographic display (Mallavarapu et al., 1999; Nabeshima et al., 1998). During phase 1, the spindle elongates to an average length of 2.5 μm. Phase 2 is characterized as a period of constant spindle length, and phase 3 is the period of rapid and dramatic spindle elongation. As the spindle elongates during anaphase (phase 3), the fluorescence intensity decreases, revealing individual microtubule behavior within the spindle. In late anaphase B, post-anaphase arrays form at the future site of the cytokinetic ring and cleavage furrow, followed by subsequent spindle collapse and cytokinesis. Owing to their spatial orientation, the post-anaphase arrays are not readily amenable to kymographic analysis and thus were not included in the following analysis.

Interphase arrays are composed of 2-3 microtubules per half bundle that behave autonomously

Previous studies of interphase microtubule arrays provided a framework for understanding the polarity, function and general behaviors of microtubule arrays as a whole (Drummond and Cross, 2000; Hagan, 1998; Mallavarapu et al., 1999; Mata and Nurse, 1997; Tran et al., 2001). However, the imaging strategies used were limited in their ability to dissect the behavior of individual microtubules within these arrays. For example, it remained unclear as to how many microtubules exist within each interphase bundle, and whether the dynamic behavior of individual microtubules within an array is coordinated. By recording images at 2-second intervals and fully utilizing the light sensitivity of our imaging system, we were able to visualize the movements of individual microtubules within cytoplasmic arrays. We have recorded over 30 cells where we can monitor the behavior of individual microtubules in each cytoplasmic bundle and have chosen the best two examples for further analysis. Our analysis of such microtubule arrays indicate that each of the cytoplasmic arrays is composed of 2-3 microtubules per half bundle, with 4-7 at the zone of overlap at the nuclear envelope. As shown in images from a time-lapse movie taken during G2 (Fig. 2A), distinct regions of increased fluorescence intensity were present along the length of one half of the microtubule bundle. The region of lowest fluorescent intensity occurs near the cell tip (marked by an arrow in Fig. 2A, time 154). In this frame, the fluorescent intensity increases at two distinct points along the length of the bundle towards the nucleus (Fig. 2A, time 154, arrowheads). This change in intensity suggests that microtubules of varying lengths exist in one bundle. In addition, the time-lapse movie (Movie 1, http://jcs.biologists.org/supplemental/) clearly shows microtubule growth towards the cell tip from each of these brighter regions, which identifies these regions as microtubule plus ends.

To demonstrate that the growth pattern we observed was owing to overlapping microtubules and not single microtubules with uneven GFP:α-tubulin incorporation, we also displayed this movie as a kymograph (Fig. 2B). A line descending from left to right in the kymograph represents an increase in microtubule length over time, whereas a line ascending from left to right (towards the SPB) represents a decrease in

Table 1. Growth and shrinkage rates of individual microtubules

	Interphase	Intra-nuclear astral	Anaphase B	Telophase	Astral
Growth	3.18±0.61 (*n*=4)	NA	0.70±0.12 (*n*=4)	NA	2.2±48 (*n*=2)
Shrinkage	16.99±2.39 (*n*=4)	20-25 (*n*=10)	2.33±0.55 (*n*=5)	7.33±0.84 (*n*=4)	9.2 (*n*=1)

All measurements are in μm/minute. *n*=number of microtubules counted.

microtubule length (marked by white arrow and black arrow respectively, Fig. 2B). The life history of an individual microtubule is represented by the triangular fluorescence pattern formed by the combination of such growth/shrinkage lines. Between periods of growth and shrinkage, the microtubule remains at the cell tip for a short period before undergoing catastrophe. This is seen on the kymograph (Fig. 2B) in the space between growth and shrinkage lines. The fluorescence patterns for individual microtubules overlap one another, demonstrating that several individual microtubules exist in each half bundle, but do not grow in unison.

To quantify our observations of microtubule number in each half-bundle, we made a plot of pixel intensity for single time points in the kymograph seen in Fig. 2B. The plots in Fig. 2C represent the pixels in one vertical pixel line (one time point) for points 154, 156 and 179 shown in Fig. 2B (also seen in Fig. 2A). These peaks correspond to the pixels on the kymograph where overlapping microtubules are seen (Fig. 2A, asterisk). After correcting for background, we determined the average intensity value for one microtubule to be 18 arbitrary units (a.u., see Materials and Methods). The average intensity for the microtubule minus-end overlap zone (Fig. 2A and 2B, asterisk) was 80 a.u., indicating that four microtubules are present here. Furthermore, at the positions where we see overlapping fluorescence regions, the intensity increased in increments of approximately 20 a.u., indicating that the increase is owing to the presence of a single additional microtubule.

Previous work has argued that, if multiple microtubules exist in interphase bundles, their presence could not be detected due to simultaneous growth and shrinkage (Drummond and Cross, 2000). Such a coordinated microtubule growth hypothesis also assumes that the continued presence of a growing microtubule end is due to multiple rounds of catastrophe and rescue by the same bundle. By contrast, our data indicates that microtubules encounter the cell tip one at a time, demonstrating that individual microtubules act autonomously. Shorter microtubules do not reach the cell tip until the previous one has already begun to depolymerize. This is illustrated in the kymograph in Fig. 2B, which first shows a microtubule depolymerizing from the cell tip. As the microtubule shrinks to about one-third of its length, the fluorescence intensity increases as this microtubule overlaps a second growing microtubule (arrowhead, Fig. 2B). This second microtubule continues to grow towards the cell tip. This alternating growth and shrinkage pattern in overlapping microtubules continues to repeat until the half bundle disappears at time 275.

Our data also provides information about the frequency of catastrophe and rescue of interphase microtubules. We show that, once catastrophe occurs, the microtubule completely depolymerizes. This is evident on the kymograph where growth and shrinkage lines for individual microtubules are continuous (Fig. 2B). In the first panel of Fig. 2A (time 154), a microtubule is near the cell tip and begins to depolymerize throughout subsequent time points (Fig. 2A, time 154 and 172, arrow). As this microtubule depolymerizes, a second overlapping microtubule continues growing until catastrophe occurs at the cell tip (Fig. 2A, time 154 and 172, arrowhead). This pattern of microtubule growth and shrinkage demonstrates the autonomy of single microtubules within the bundle. The majority of microtubules never experience a catastrophe before they reach the end of the cell, and do not undergo a rescue once a catastrophe has occurred. However, at later time points, some microtubules undergo a catastrophe before hitting the cell tip. This is evident in the time-lapse movie in which a small half bundle of three microtubules oriented along the cell axis exhibits this behavior (Movie 1, http:// jcs.biologists.org/supplemental/). Additionally, there are a few short microtubules nucleated at the SPB that are not part of the organized bundles. These microtubules experience a more rapid growth and shrinkage cycle (small triangles in middle of kymograph). Although shorter, these additional microtubules still have only one growth and shrinkage cycle during their lifetime.

The kymographs were also used to measure rates of microtubule polymerization and depolymerization. From this analysis, we have found that microtubules in the interphase arrays have growth rates of 3.18±0.61 μm/minute and depolymerization rates of 16.99±2.39 μm/minute (Table 1), which is consistent with previously published reports (Behrens and Nurse, 2002; Drummond and Cross, 2000).

Growth of new interphase microtubules is inhibited upon the transition to mitosis

The transition from interphase to mitosis (G2/M) is marked by a dramatic change in microtubule organization and dynamics. Fission yeast have a closed mitosis and, as a consequence, both cytoplasmic and nuclear microtubules remain in separate cellular compartments. Cytoplasmic microtubule arrays disappear as the mitotic spindle forms and reappear as astral microtubules during anaphase. Two possible mechanisms could explain the disappearance of cytoplasmic microtubule arrays at the G2/M transition. Either the depolymerization of interphase arrays is promoted upon entry into M or, alternatively, the growth of new microtubules could be restricted whereas existing microtubules complete a normal growth and shrinkage cycle. These two scenarios can be distinguished based on the length of time that existing microtubules persist once spindle formation begins.

Our results support the second scenario, wherein the existing cytoplasmic microtubules persist briefly after the mitotic spindle has formed; yet the formation of new cytoplasmic microtubules is severely reduced (Fig. 3). When GFP:α-tubulin fluorescence first appears at the SPB (a marker of entry into

mitosis) (Fig. 3A, arrow), any microtubule bundles not associated with the SPB finish their growth to the cell tip but are not replaced by new microtubules. The cytoplasmic bundles directly associated with the SPB undergo several additional cycles of microtubule initiation and catastrophe. Occasionally, a new cytoplasmic microtubule will be initiated during phase 1 of spindle growth (Fig. 3). These events are rare and only occur at the SPB. Moreover, each newly initiated bundle has a shorter growth period than the previous bundle. The last bundle to form in Fig. 3 is composed of two microtubules as seen in the kymograph in Fig. 3B. The longer microtubule grows along most of the length of the cell before it undergoes catastrophe (Fig. 3B, arrow), whereas the other only grows about half this length (Fig. 3B, arrowhead). Cytoplasmic microtubules initiated after the start of mitosis rarely reach the cell tip before they depolymerize. In summary, we find that progression of microtubule loss occurs first by a loss of nucleation at non-SPB microtubule nucleation sites on the nuclear envelope (Tran et al., 2001), followed by a decrease in the frequency of initiation and a period of growth of microtubules from the SPB.

Highly dynamic intra-nuclear microtubules and the mitotic spindle replace organized cytoplasmic microtubule arrays

Fission yeast spindles share many structural similarities with those of metazoan cells, including the presence of multiple microtubules attached to each kinetochore. Therefore, we chose to monitor individual microtubules in the *S. pombe* spindle to identify similarities in the spindle assembly process that might be shared by *S. pombe* and metazoan cells. We found that, similar to metazoan cells, a dramatic increase in microtubule dynamics occurred in the *S. pombe* nucleus upon the onset of mitosis. Nucleation of short microtubules that displayed rapid cycles of polymerization and depolymerization was initiated on the nuclear face of the SPB, concurrent with the disappearance of cytoplasmic arrays. These intra-nuclear astral (INA) microtubules appeared before the formation of the bipolar mitotic spindle inside the nucleus. We have determined the intra-nuclear localization of these microtubules using projections through the nucleus, as seen in Fig. 4A. Additionally, we have seen nuclear localization of INA microtubules in cells expressing GFP:cytochrome P450 reductase (YY106), a nuclear envelope marker (data not shown). We have observed INA microtubules in over 30 cells. Owing to the technical difficulties in filming them, we have used five movies for further analysis. Two movies are represented in these figures. Because of the rapid turnover of these microtubules (average half-life=4 seconds, their optimal detection required capturing images at 2-second intervals. We believe that the rapid dynamics exhibited by INA microtubules are essential for their function during early mitosis, as with the change in dynamics in metazoan cells.

Because INA microtubules appear during the earliest stages of mitosis, we wanted to determine if they were present in later mitotic stages. We observed that INA microtubule activity is restricted to pre-anaphase mitosis, which indicates that the presence of INA microtubules is regulated by the cell cycle. INA microtubules extend from the SPB prior to spindle assembly and disappear late in phase 2 before anaphase

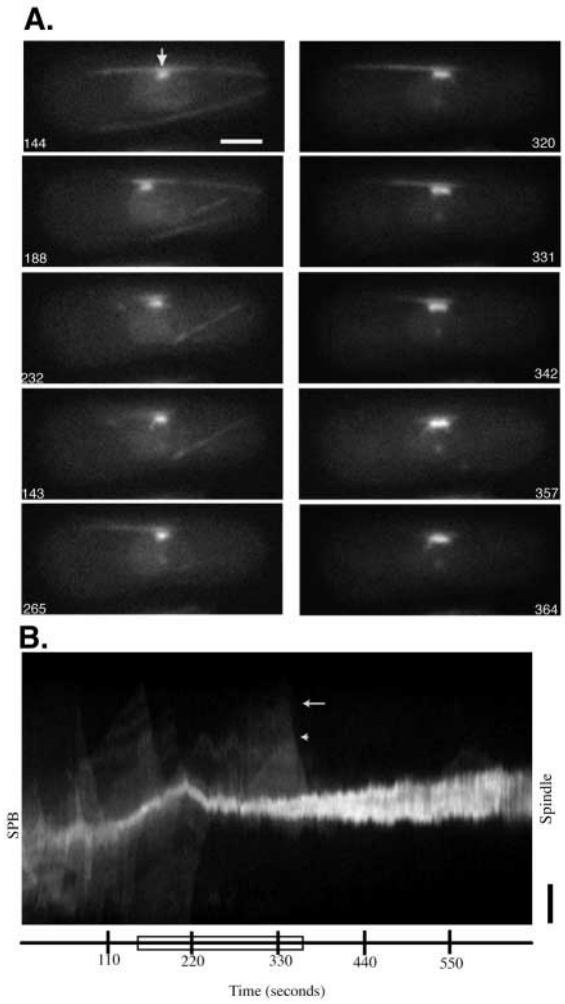

Fig. 3. At the G2-M transition, cytoplasmic microtubules disappear as the spindle forms inside the nucleus. (A) Shown here are still images from a time-lapse movie of a cell entering mitosis. The cell shown here is strain 2694 expressing both GFP:α-tubulin and GFP:Swi6, a heterochromatin binding protein (Pidoux et al., 2000). The early spindle is seen as a small bar of fluorescence near the SPB on the inside of the nucleus (arrow, time 144). As mitosis progresses, the cytoplasmic bundles at the SPB persist whereas other nuclear-associated microtubules disappear (time 265). When the spindle reaches a length of approximately 1.0 μm, the cytoplasmic bundles at the SPB have also disappeared (time 342). These images are representative of the time points marked by the rectangle on the time line of the kymograph in B. Bar, 2 μm. (B) The kymograph is made from the same time-lapse movie shown in A. Cytoplasmic microtubules are seen as triangular projections extending from the SPB (as in Fig. 2). The pattern becomes much less complex around time point 110 as additional cytoplasmic bundles disappear. At time 230, microtubule growth is restricted to one side of the SPB. Once the phase 1 spindle has formed, the cytoplasmic microtubules become progressively shorter as seen by the decreasing length of the growth lines shown by the arrow and arrowhead. Cytoplasmic microtubules are gone by the time the spindle reaches a length of 1.0 μm (time 265). Bar, 2 μm.

begins. In Fig. 4A (see also Movie 2, http:// jcs.biologists.org/supplemental/), a single cell is shown progressing from G2 to M. To detect the maximum number and the earliest occurrence of INA microtubules, these images were taken at 7-second

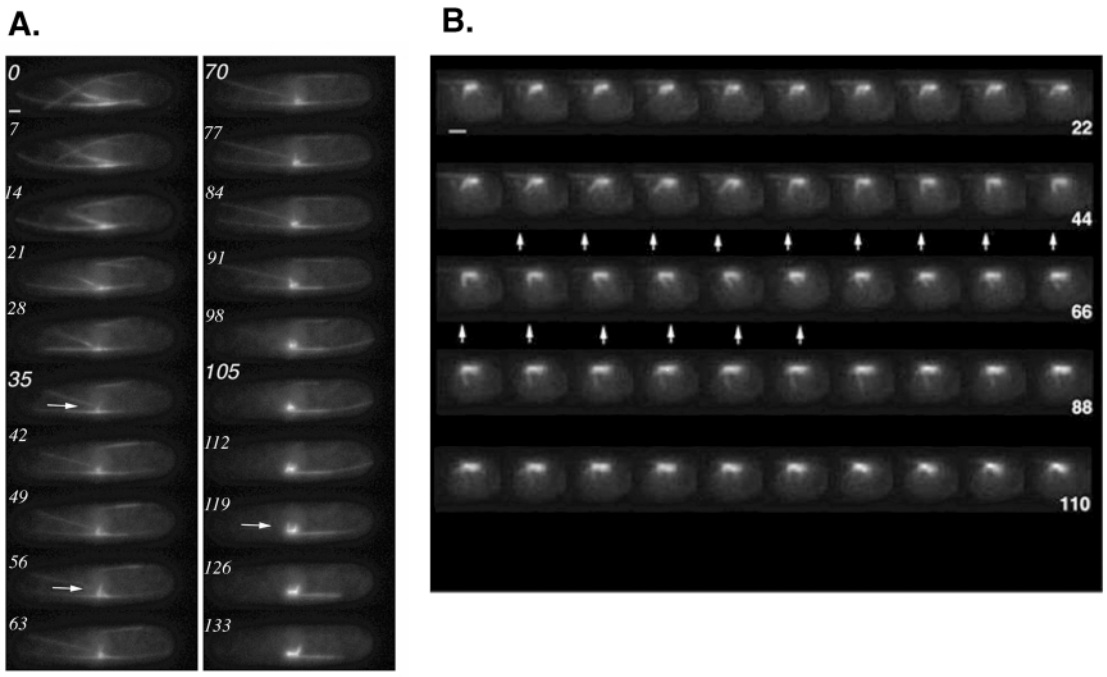

Fig. 4. Short dynamic microtubules are part of the early spindle. (A) INA microtubules appear at the earliest stages of spindle assembly. These still images are projections of three 0.4μm sections taken at 7-second intervals (strain, YY105). The fluorescent bar is the short spindle. The arrow at time point 35 shows the earliest detected INA microtubule before any visible spindle pole separation has occurred. The arrow at time 56 shows the same INA microtubule that has elongated towards the nuclear center. The arrow at time 119 shows two INA microtubules after spindle pole separation, one extending from each spindle pole. Bar, 1 μm (see Movie 2, http://jcs.biologists.org/supplemental/). (B) Sequential images of a single nucleus with an early phase 1 spindle and INA microtubules taken at approximately 2-second intervals. The arrows follow a single INA microtubule bundle as it sweeps across the nucleus. The same microtubule stops sweeping and appears to grow in length over the next several time frames. The cells in both A and B progressed normally through anaphase. Bar, 1 μm (see Movie 3, http://jcs.biologists.org/supplemental/).

intervals and represent a 3D projection of three optical sections. Using these projections we were able to describe the general patterns of INA movement in multiple focal planes. INA microtubules appear when GFP:α-tubulin fluorescence is first observed on the SPBs, and before any measurable SPB separation occurs (Fig. 4A, arrow at time 35). INA microtubules are short projections protruding from the SPB extending towards the center of the nucleus. The initial INA microtubules were less than 1 μm long and were perpendicular to the nuclear face of the SPB. As the spindle elongated, the distance between individual INA microtubules also increased, indicating that each spindle pole has associated INA microtubules (Fig. 4A, time 119, arrow).

To determine whether INA microtubule activity is cell-cycle dependent, we assessed the amount of INA microtubule activity relative to progression through mitosis. Although INA microtubules remain active during prophase and prometaphase, their number diminishes over time. INA microtubules are last observed just before phase 2. We identified the last frame of the time-lapse movie where INA microtubules are seen and marked the corresponding time point on a kymograph (data not shown). This time point is at the metaphase to anaphase transition.

INA microtubules exhibit a dramatic lateral movement within the nucleus. Often two or more microtubules were initiated at the same pole with each bundle sweeping in opposite directions (Fig. 4B; see also Movie 3, http://jcs.biologists.org/supplemental/). A rapid change in the number and position of INA microtubules was observed between frames. Notably, we found one hyper-stable INA microtubule on the left-hand pole of the spindle (Fig. 4B, indicated by arrows in second and third rows). This hyper-stable INA microtubule moved with a sweeping motion as it passed from an outward orientation towards the nuclear envelope on the left, to a final position oriented toward the center of the nucleus (see Movie 3, http://jcs.biologists.org/supplemental/). The arrows in Fig. 4B mark the path of the microtubule as it moved from left to right. To verify that INA microtubules actually sweep, we also made a time-lapse movie with three optical sections at 1-second intervals (data not shown). INA microtubules in these videos consistently exhibited a sweeping motion. Although we cannot exclude the possibility that the sweeping motion is due to rapid sequential polymerization, the rates of growth and shrinkage required for such behavior would be far greater then any previously measured rates for microtubule dynamics in vivo and is an unlikely explanation for our observations.

Rapid microtubule polymerization and depolymerization is another striking feature of INA microtubules. Lengths of INA microtubules range from 0.2 μm to 1.2 μm. The number of INA microtubules in any one frame is highly variable and the overall pattern of appearance and persistence of these microtubules appears to be random. Generally, there are only one or two microtubules observed per frame (Fig. 4), although occasionally three or more microtubules appear in interspersed frames. In the first five frames (11 seconds) in the recording

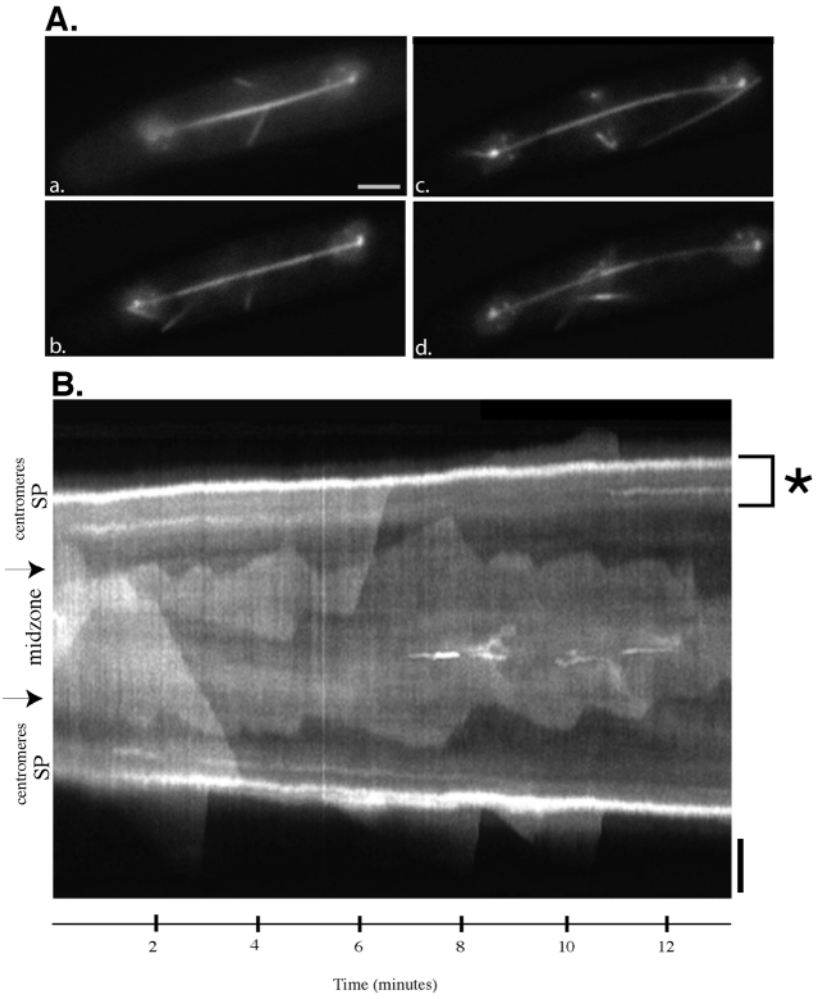

Fig. 5. During anaphase B, microtubule plus ends are dynamic but do not show depolymerization at minus ends. (A) Images of anaphase B spindle elongation. The region of overlap between the two half spindles gradually decreases as the spindle elongates. The strain used here is 2694. The GFP:Swi6-stained centromeres mark the location of the spindle poles in each daughter nucleus. Bar, 2 μm. (B) Kymograph of the anaphase B time-lapse movie seen in A. The increased fluorescence in the center of the kymograph, delineated by arrows, reflects the overlap of oppositely oriented polar microtubule plus ends. The triangular patterns reflect the growth and shrinkage of individual microtubules. The asterisk marks the distance between unique fluorescence patterns in the spindle microtubules due to uneven incorporation of GFP:α-tubulin and the bright spindle pole labeled by GFP:Swi6 at the centromeres. This distance remains constant as the spindle elongates. SP, spindle pole; midzone, zone of overlap of antiparallel microtubules. Bar, 2 μm.

shown in Fig. 4B, only two bundles were present, one at each pole. In the next seven frames (or 15.4 seconds), three or more bundles were apparent, although most were partially out of the plane of focus. Most INA microtubule bundles were transient, persisting for fewer than 10 seconds, with a significant number of these only lasting for 4 seconds. However, a few microtubules (two out of a total of 67) appeared to be more stable, lasting over 60 seconds.

INA microtubules are much more dynamic than any other microtubule array previously observed in fission yeast. Given that microtubules 0.2-0.5 μm long can disappear during the 2 seconds between frames, we were able to determine that INA microtubules are capable of depolymerizing at rates of approximately 15-20 μm/minute. The measurement of INA microtubules persisting long enough to be detected on a kymograph also yielded depolymerization rates in this range, up to a maximum of 25 μm/minute (n=10, Table 1).

Microtubule plus ends at the spindle midzone in anaphase B undergo catastrophe and rescue

In order to determine whether individual spindle microtubules have autonomous behaviors, we examined microtubules at the metaphase to anaphase transition. The overall fluorescence of the metaphase spindle was too bright to allow detection of individual microtubules within the spindle. We have visualized oscillations of GFP:Swi6-tagged centromeres along the length of the spindle that suggests kinetochore microtubules in metaphase spindles having dynamic plus ends (data not shown). Our data supports earlier studies of metaphase microtubule dynamics using fluorescence recovery after photobleaching (FRAP) (Mallavarapu et al., 1999).

As the spindle elongates during anaphase B, the overall fluorescence intensity of the spindle decreases as kinetochore microtubules shorten to the poles and the extent of microtubule overlap decreases. This allows us to monitor the behavior of individual microtubules remaining in the spindle midzone. The decreasing overlap zone is shown in the panels of Fig. 5A. As demonstrated by the kymograph in Fig. 5B, the plus ends of spindle microtubules in the midzone experienced sequential catastrophe and rescue events. By contrast, microtubules in the interphase cytoplasmic arrays do not rescue once they have undergone catastrophe. As measured by kymographic analysis (see Materials and Methods), we determined the growth rates of spindle microtubules to be 0.70±0.12 μm/minute and the shrinkage rates were 2.33±0.55 μm/minute (Table 1).

Late anaphase spindle microtubules do not show evidence of tubulin subunit exchange at both ends. Uneven incorporation of GFP:α-tubulin into microtubule polymers created a striped pattern in the kymograph. These stripes provide positional markers along the length of the microtubule. Strikingly, these patterns slope outwards at the same rate as the spindle poles (Fig. 5B, asterisk). If subunits were being lost at the minus end, these stripes would move towards the spindle poles and subsequently disappear. Instead, the distance between the stripes and the spindle poles remains constant throughout anaphase.

Telophase spindle collapse occurs by a sequence of individual depolymerizing microtubules

The mechanism of spindle disassembly in telophase remains poorly understood. Spindle collapse can be described by the order in which microtubules of the two half spindles

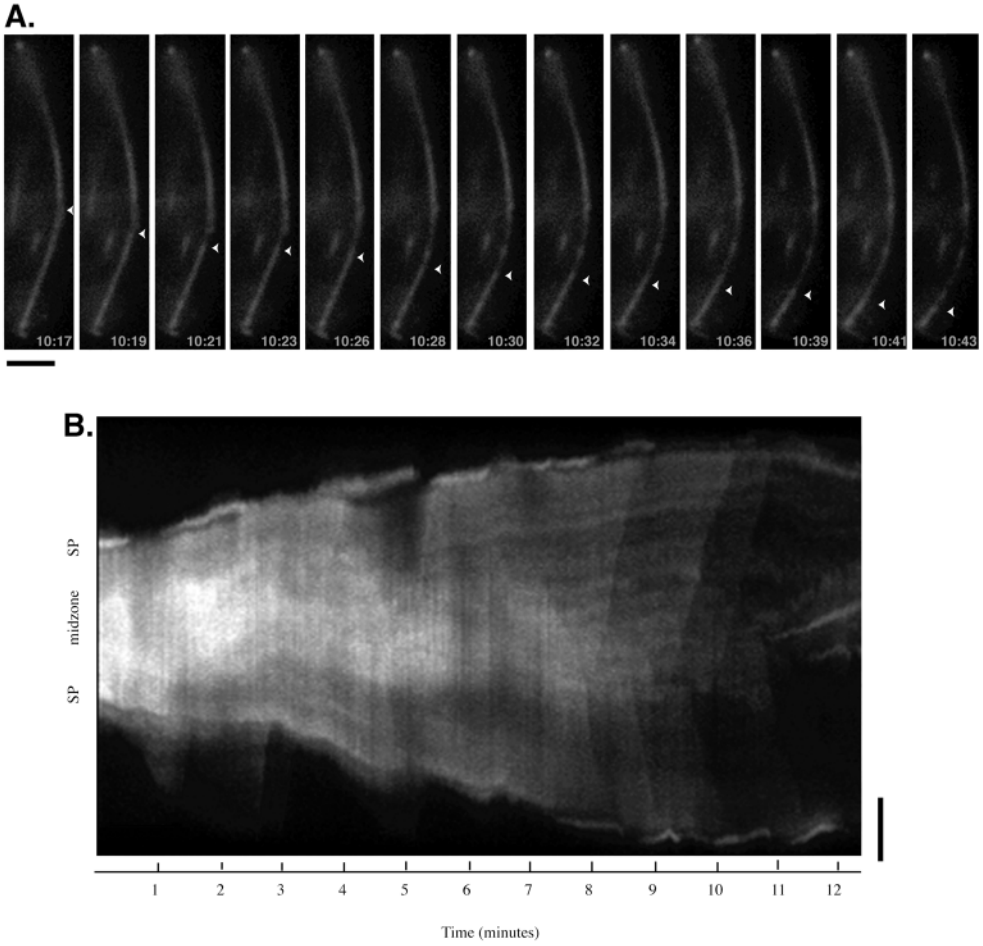

Fig. 6. Spindle collapse occurs by sequential depolymerization of oppositely oriented microtubules. (A) A single microtubule is shown depolymerizing toward the lower spindle pole. The still images are sequential images taken at approximately 2-second intervals over 26 seconds. The arrowhead points to the plus end of the depolymerizing microtubule. Bar, 2 μm. (B) The same time-lapse movie is shown as a kymograph. The kymograph shows anaphase B spindle elongation and spindle collapse. After the spindle stops elongating (time 7 minutes), the microtubules begin to depolymerize one by one. This appears as a series of parallel lines sloping toward the spindle poles in an alternating pattern. Successive depolymerization lines are parallel, showing that rates of depolymerization are the same for each microtubule. SP, spindle pole; midzone, zone of antiparallel microtubule overlap Bar, 2 μm (see Movie 4, http://jcs.biologists.org/supplemental/).

depolymerize. Either the entire spindle collapses simultaneously or, alternatively, spindle collapse occurs via the sequential depolymerization of individual microtubules. During other stages of the cell cycle, we found that individual microtubules behave autonomously, raising the expectation of finding the same behavior during mitotic spindle breakdown. Our data demonstrates that individual microtubules depolymerize from their plus ends towards the SPB in collapsing spindles (Fig. 6; see also Movie 4, http://jcs.biologists.org/supplemental/). A striking pattern of alternating single microtubule depolymerization, first from one half of the spindle and then the other, is repeated until the spindle has completely disassembled and the post-anaphase array has formed. Fig. 6A shows sequential images of the depolymerization of a single microtubule from the midzone towards the SPB at the bottom of the image. The arrowhead indicates a spot of increased fluorescence, marking the tip of the depolymerizing microtubule.

This highly coordinated ordering of microtubule depolymerization is highlighted in the kymographic analysis (Fig. 6B). In the telophase spindle, the spindle midzone (roughly a third of the total spindle length) is significantly brighter than the regions closer to the spindle poles due to the overlapping microtubules. Individual depolymerizing microtubules are seen as lines sloping to the right and towards the spindle poles. These lines originate at the spindle midzone and terminate at the spindle pole. As each microtubule leaves the bipolar array, the overall intensity of the spindle fluorescence diminishes. As demonstrated in both the movie and the resulting kymograph, the next microtubule began to depolymerize before the previous one had completely disappeared. The number of lines we see in the kymograph (8) is consistent with published electron microscopy (EM) results showing that late anaphase spindles contain upwards of 12 polar microtubules (Ding et al., 1993). Some of the spindle microtubules persist after spindle collapse is complete, accounting for the remaining microtubules (Movie 4, http://jcs.biologists.org/supplemental/). The depolymerization lines are strikingly parallel; each line has the same slope, indicating that the rate of microtubule depolymerization is constant (7.3±0.84 μm/minute, Table 1).

Astral microtubules exhibit similar dynamics to cytoplasmic interphase microtubules

Astral microtubules are the first cytoplasmic microtubules to reappear after the onset of mitosis. For this reason, we sought to determine whether the astral microtubule arrays behave more like spindle microtubules or cytoplasmic interphase arrays in terms of frequency of catastrophe and rescue, and rates of polymerization and depolymerization. The astral microtubules, when displayed in a kymograph, form the same growth triangles oriented towards the cell periphery as the interphase arrays (Fig. 7). The overlapping pattern of growth triangles again demonstrates that astral arrays are bundles composed of multiple microtubules. In addition, each microtubule has only one cycle of growth and shrinkage. Measurements of the growth rate of individual microtubules

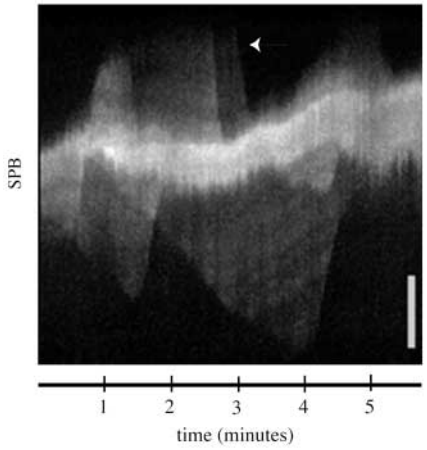

Fig. 7. Mitotic cytoplasmic astral microtubules behave like cytoplasmic interphase bundles. This kymograph is from a time-lapse movie of astral microtubule growth and shrinkage during anaphase B. It shows there are multiple microtubules in a bundle (arrow). Each individual microtubule only undergoes one growth and catastrophe cycle. SPB, spindle pole body. Bar, 2 μm.

indicate that their dynamics are similar to interphase arrays (Table 1) with a growth rate of 2.2±48 μm/minute and shrinkage rates of 9.2 μm/minute. Greater similarity is observed between astral microtubules and cytoplasmic arrays than astral microtubules and other mitotic arrays such as the INA microtubules.

Discussion

Observations of individual microtubule dynamics within the context of larger microtubule arrays provide a more fundamental understanding of how these arrays are regulated. Previous studies of microtubules in fission yeast have focused on identifying the overall dynamics of these arrays. The goal of our study was to define the behavior of individual microtubules in each array, to compare their polymerization and depolymerization rates, the frequency of catastrophe and rescue, and the levels at which the behavior of individual microtubules are coordinated. Evaluating these parameters will subsequently allow for a better evaluation of how MAPs and motor proteins organize and regulate the behavior of different populations of microtubules.

In summary, we have shown that cytoplasmic microtubules exhibit similar properties in terms of rates of growth and shrinkage, and frequency of catastrophe and rescue, independent of the cell cycle. By contrast, rates of growth and shrinkage of nuclear microtubules are highly variable during mitosis. Spindle microtubules have slower growth and shrinkage rates compared with cytoplasmic interphase microtubules (Table 1). This is in contrast to the findings in mammalian cells where only the frequency of catastrophe and rescue changed during mitosis, whereas growth and shrinkage rates remained constant (Rusan et al., 2001). However, *S. pombe* is similar to Newt Lung tissue culture cells and budding yeast. In these cells, microtubule polymerization/depolymerization rates decreased in cells that had entered mitosis (Rusan et al., 2001; Tirnauer et al., 1999). The INA microtubules are an exceptional class as they are the only microtubules during mitosis that show an increase in polymerization/depolymerization rates compared with cytoplasmic microtubules.

Interphase cytoplasmic arrays are composed of autonomous microtubules that gradually decrease in number upon the transition to mitosis

Previous work has established that interphase microtubule arrays are composed of bundles of microtubules arranged in an antiparallel fashion with their minus ends overlapping at the SPB or at ectopic nucleation sites on the nuclear envelope, and their plus ends extending towards the cell cortex (Drummond and Cross, 2000; Tran et al., 2001). In these studies, the fluorescent intensity of the interphase arrays, as measured using a GFP:α-tubulin strain, was determined to have a three-fourfold increase in the 'overlapping' region near the SPB as compared with the outward-facing plus ends. These data were interpreted to suggest that the arrays have one microtubule growing in each direction with two antiparallel overlapping microtubules in the middle. It was also assumed that the continued presence of a growing microtubule end is owing to multiple rounds of catastrophe and rescue. However, this apparently straightforward interpretation is in disagreement with EM studies that show cross-sections of 3-5 microtubules overlapping at the SPB, and clusters of 1-4 microtubules in the cytoplasm of G2 cells (Ding et al., 1997).

In our study, we present new observations of interphase microtubule dynamics (Fig. 2) that are consistent with an arrangement of multiple microtubules in each half bundle with their minus ends proximal to the SPB and their plus ends growing toward the cell cortex. These new studies are consistent with previous EM studies (Ding et al., 1997). Although the rates of growth and shrinkage of individual microtubules within a bundle are the same, the dynamics of individual microtubules are not coordinated.

Interphase cytoplasmic arrays play important roles in intracellular transport, organelle positioning and polarized (tip) growth (Mata and Nurse, 1997; Tran et al., 2001; Yaffe et al., 1996). The proteins Tea1, Tea2 and Tip1 form a plus-end-binding complex that regulates the growth of interphase microtubules and plus-end tip growth (Behrens and Nurse, 2002; Browning et al., 2000; Brunner and Nurse, 2000; Mata and Nurse, 1997). In light of our analysis, it appears that they act on single microtubules instead of a microtubule bundle.

Microtubules depolymerize in the cytoplasm and repolymerize in the nucleus upon the transition to mitosis. Microtubule dynamics during the transition to mitosis (Fig. 3) support a model in which the breakdown of cytoplasmic microtubules does not result from an increase in the frequency of depolymerization, but rather a reduction in the number of new microtubules being nucleated. As the spindle begins to form in the nucleus, only cytoplasmic bundles associated with the SPB remain. These cytoplasmic microtubules undergo a few additional rounds of growth and shrinkage although, in later cycles, microtubules do not reach the ends of the cell. This process could be controlled by several mechanisms, including regulation by the concentration of available tubulin dimers or active depolymerization under cell-cycle control. Since spindle

microtubules are readily assembled in the nucleus, the depletion of tubulin dimers in the cytoplasm would affect the ability of the ectopic (i.e. non-SPB) nucleation sites and eventually the SPB to support new microtubule growth. Our observation that the new cytoplasmic microtubules initiated at the SPB do not achieve their full length before undergoing a catastrophe would support this model. A second possibility is that the ectopic nucleation sites are cell-cycle regulated and are inactivated at the transition to mitosis. The decrease in overall cytoplasmic microtubule growth could be attributed to a decrease in the activity of growth-promoting factors or an increased activity of microtubule growth inhibitors in the cytoplasm. Candidates for regulatory proteins include: Mal3, the *S. pombe* EB1 homolog; one of the end-binding proteins Tea1, Tea2 or Tip1; or Alp14 and Dis1, the fission yeast homolog of *Xenopus* XMAP215; and Klp2 (Behrens and Nurse, 2002; Browning et al., 2000; Brunner and Nurse, 2000; Chen et al., 2000; Garcia et al., 2001; Nabeshima et al., 1995; Nakaseko et al., 2001; Popov et al., 2001; Tirnauer and Bierer, 2000; Troxell et al., 1997).

INA microtubules are a novel class of dynamic microtubules in fission yeast

The discovery of a dynamic class of microtubules in the prometaphase and metaphase fission yeast spindle has important implications for understanding spindle formation and chromosome attachment. Previously, EM analysis identified short microtubules associated with the nucleoplasmic face of the SPB that are not part of the central spindle (Ding et al., 1993; Tanaka and Kanbe, 1986). The presence of these microtubules was not readily detected in other studies because analysis of their dynamic properties requires rapid imaging in real time. On the basis of our analysis of the behavior of INA microtubules, we suggest that INA microtubules act as the precursors to other functional classes of spindle microtubules.

The intrinsically unstable INA microtubules acquire a functional role upon interaction with extrinsic nuclear factors. Such interactions would change the dynamics of INA microtubules, causing them to become stabilized. The sweeping and probing behaviors of INA microtubules and their dynamic activity early in mitosis make them ideal candidates for involvement in search and capture mechanisms for chromosome attachment to the spindle. Kinetochore attachments would stabilize INA microtubules as components of the kinetochore bundle. In addition, sweeping INA microtubules might play a role in chromosome congression, thus ensuring proper chromosome segregation in anaphase A.

INA microtubules might act as building blocks of the spindle. Of the nine kinesin-like proteins (Klps) present in *S. pombe*, three of the mitotic Klps present during mitosis, Cut7, SpKid and Pkl1 are known to influence spindle assembly (Hagan and Yanagida, 1995; Pidoux et al., 1996) (J. Paluh and W.Z.C., unpublished). Cut7p is a BimC family Klp needed for bipolar spindle formation during phase1 (Hagan and Yanagida, 1990). In *cut7 ts* alleles at the nonpermissive temperature, the initial interdigitation of microtubules extending obliquely from the half spindles fails, and the SPBs are unable to separate. The bipolar array could be assembled through sequential interactions of oppositely oriented INA microtubules that are stabilized by Cut7. Pkl1 could further affect their dynamics. The chromokinesin SpKid appears to be involved in establishing the antiparallel organization of microtubules at the spindle midzone and in aligning chromosomes at the metaphase plate (J. Paluh and W.Z.C., unpublished). SpKid might also interact with INA microtubules to promote their stabilization upon their interaction with chromatin or with antiparallel microtubules from the other SPB. Finally, INA microtubules might help to position the mitotic spindle within the nucleus. This function would be analogous to interphase microtubules that exert pushing forces on the nucleus to position it in the center of the cell preceding mitosis (Tran et al., 2001).

Anaphase spindle microtubules have dynamic plus ends but do not exhibit minus-end dynamics

The spindle of *S. pombe* is composed of 3-4 kinetochore microtubules per kinetochore and 12-14 antiparallel microtubules in each half spindle (Ding et al., 1993). This relatively small number of microtubules makes it possible to visualize individual microtubules in the spindle. Loss of kinetochore microtubules and some polar microtubules occurs throughout anaphase (Fig. 6) and reduces the number of microtubules in the central spindle to a total of 12 (Ding et al., 1993). As the spindle elongates during anaphase B, the overall fluorescence intensity subsequently decreases as the region of microtubule overlap becomes restricted to the midzone. These factors decrease the intensity of the GFP:α-tubulin sufficiently that the uneven incorporation of GFP:α-tubulin into spindle microtubules becomes visible. As the spindle elongates, the regions of varying fluorescence intensity remain constant with respect to the spindle poles. Our observations are supported by previous FRAP studies, which showed no recovery in the photobleached area of an anaphase spindle (Mallaparavu et al., 1999). In total, these data are inconsistent with the minus-end depolymerization in anaphase microtubules, whereas flux is seen in vitro in vertebrates and in kinetochore microtubules of *Drosophila* embryos (Maddox et al., 2000; Mitchison, 1989; Sawin and Mitchison, 1994). Similar to budding yeast, microtubule assembly and disassembly in anaphase appears to occur exclusively at microtubule plus ends (Maddox et al., 2000). Similar measurements were not possible in metaphase spindles owing to the amount of total fluorescence in the tightly packed spindle.

Pairs of oppositely oriented microtubules are a major stabilizing force in late mitotic spindles

Two alternative scenarios could account for spindle collapse at the end of telophase. First, loss of integrity of the spindle midzone at the plus ends of microtubules might occur when overlapping microtubules are no longer stabilized by crosslinking proteins, leading to simultaneous depolymerization. This mechanism would result from the rapid degradation of stabilizing proteins such as Cut7 or Dis1 (Hagan and Yanagida, 1992; Nabeshima et al., 1998). Alternatively, stabilizing forces could decrease gradually. Our observations of spindle dynamics (Fig. 6) support this latter scenario. From EM studies of mitotic spindles, the microtubules in telophase spindles are packed tightly in a square conformation (Ding et

al., 1993). The peripheral microtubules with fewer lateral interactions would be the first to depolymerize followed by the internal microtubules, as bonds with the adjoining external microtubules are broken. The alternating pattern of microtubule depolymerization that we observed supports the notion that the stabilizing forces between pairs of oppositely oriented microtubules is important for maintaining spindle integrity.

Astral microtubules found on the cytoplasmic face of the SPB closely resemble the interphase arrays in terms of their polymerization and depolymerization rates, organization and behavior (Fig. 7, Table 1). We propose that their similar dynamics are a result of existing in a similar environment and performing similar functions as interphase cytoplasmic microtubules. Thus, whereas interphase microtubules help position the nucleus, astral microtubules help to orient the spindle axis relative to the cell axis (Oliferenko and Balasubramanian, 2002; Tran et al., 2001).

In summary, using enhanced methods of detection has led to a more precise characterization of microtubule arrays in fission yeast by highlighting the behaviors of individual microtubules within these arrays. This analysis lays the groundwork for a more insightful interpretation of how proteins function in the cell to affect microtubule dynamics or are themselves affected by microtubule dynamics. Future experiments should emphasize the identification of the mechanism by which mutations in MAPs and motor proteins affect individual microtubule dynamics.

We thank Ian Cheeseman, Janet Paluh and Scott Dawson for helpful discussions about this manuscript. This research was support by a grant from the National Institutes of Health and the Torry Mesa Research Institute-Syngenta Biotechnology, San Diego.

References

Behrens, R. and Nurse, P. (2002). Roles of fission yeast tea1p in the localization of polarity factors and in organizing the microtubular cytoskeleton. *J. Cell Biol.* **157**, 783-793.

Browning, H., Hayles, J., Mata, J., Aveline, L., Nurse, P. and McIntosh, J. R. (2000). Tea2p is a kinesin-like protein required to generate polarized growth in fission yeast. *J. Cell Biol.* **151**, 15-28.

Brunner, D. and Nurse, P. (2000). CLIP170-like tip1p spatially organizes microtubular dynamics in fission yeast. *Cell* **102**, 695-704.

Chen, C. R., Chen, J. and Chang, E. C. (2000). A conserved interaction between Moe1 and Mal3 is important for proper spindle formation in *Schizosaccharomyces pombe*. *Mol. Biol. Cell* **11**, 4067-4077.

Ding, D.-Q., Chikashige, Y., Haraguchi, T. and Hiraoka, Y. (1998). Oscillatory nuclear movement in fission yeast meiotic prophase is driven by astral microtubules, as revealed by continuous observation of chromosomes and microtubules in living cells. *J. Cell Sci.* **111**, 701-712.

Ding, R., McDonald, K. L. and McIntosh, J. R. (1993). Three-dimensional reconstruction and analysis of mitotic spindles from the yeast, *Schizosaccharomyces pombe*. *J. Cell Biol.* **120**, 141-151.

Ding, R., West, R. R., Morphew, M., Oakley, B. R. and McIntosh, J. R. (1997). The spindle pole body of *Schizosaccharomyces pombe* enters and leaves the nuclear envelope as the cell cycle proceeds. *Mol. Biol. Cell* **8**, 1461-1479.

Drummond, D. R. and Cross, R. A. (2000). Dynamics of interphase microtubules in *Schizosaccharomyces pombe*. *Curr. Biol.* **10**, 766-775.

Egel, R., Willer, M., Kjaerulff, S., Davey, J. and Nielsen, O. (1994). Assessment of pheromone production and response in fission yeast by a halo test of induced sporulation. *Yeast* **10**, 1347-1354.

Garcia, M. A., Vardy, L., Koonrugsa, N. and Toda, T. (2001). Fission yeast ch-TOG/XMAP215 homologue Alp14 connects mitotic spindles with the kinetochore and is a component of the Mad2-dependent spindle checkpoint. *EMBO J.* **20**, 3389-3401.

Hagan, I. M. (1998). The fission yeast microtubule cytoskeleton. *J. Cell Sci.* **111**, 1603-1612.

Hagan, I. M. and Hyams, J. S. (1988). The use of cell division cycle mutants to investigate the control of microtubule distribution in the fission yeast *Schizosaccharomyces pombe*. *J. Cell Sci.* **89**, 343-357.

Hagan, I. M. and Petersen, J. (2000). The microtubule organizing centers of *Schizosaccharomyces pombe*. *Curr. Top. Dev. Biol.* **49**, 133-159.

Hagan, I. and Yanagida, M. (1990). Novel potential mitotic motor protein encoded by the fission yeast cut7+ gene. *Nature* **347**, 563-566.

Hagan, I. and Yanagida, M. (1992). Kinesin-related cut7 protein associates with mitotic and meiotic spindles in fission yeast. *Nature* **356**, 74-76.

Hagan, I. and Yanagida, M. (1995). The product of the spindle formation gene sad1+ associates with the fission yeast spindle pole body and is essential for viability. *J. Cell Biol.* **129**, 1033-1047.

Hayden, J. H., Bowser, S. S. and Rieder, C. L. (1990). Kinetochores capture astral microtubules during chromosome attachment to the mitotic spindle: direct visualization in live newt lung cells. *J. Cell Biol.* **111**, 1039-1045.

Heitz, M. J., Petersen, J., Valovin, S. and Hagan, I. M. (2001). MTOC formation during mitotic exit in fission yeast. *J. Cell Sci.* **114**, 4521-4532.

Horio, T. and Hotani, H. (1986). Visualization of the dynamic instability of individual microtubules by dark-field microscopy. *Nature* **321**, 605-607.

Inoue, S. and Salmon, E. D. (1995). Force generation by microtubule assembly/disassembly in mitosis and related movements. *Mol. Biol. Cell* **6**, 1619-1640.

Maddox, P. S., Bloom, K. S. and Salmon, E. D. (2000). The polarity and dynamics of microtubule assembly in the budding yeast *Saccharomyces cerevisiae*. *Nat. Cell Biol.* **2**, 36-41.

Mallavarapu, A., Sawin, K. and Mitchison, T. (1999). A switch in microtubule dynamics at the onset of anaphase B in the mitotic spindle of *Schizosaccharomyces pombe*. *Curr. Biol.* **9**, 1423-1426.

Mata, J. and Nurse, P. (1997). tea1 and the microtubular cytoskeleton are important for generating global spatial order within the fission yeast cell. *Cell* **89**, 939-949.

Mitchison, T. J. (1989). Polewards microtubule flux in the mitotic spindle – evidence from photoactivation of fluorescence. *J. Cell Biol.* **109**, 637-652.

Moreno, S., Klar, A. and Nurse, P. (1991). Molecular genetic analysis of fission yeast *Schizosaccharomyces pombe*. *Methods Enzymol.* **194**, 795-823.

Nabeshima, K., Kurooka, H., Takeuchi, M., Kinoshita, K., Nakaseko, Y. and Yanagida, M. (1995). P93-dis1, which is required for sister chromatid separation, is a novel microtubule and spindle pole body-associating protein phosphorylated at the Cdc2 target sites. *Genes Dev.* **9**, 1572-1585.

Nabeshima, K., Nakagawa, T., Straight, A. F., Murray, A., Chikashige, Y., Yamashita, Y. M., Hiraoka, Y. and Yanagida, M. (1998). Dynamics of centromeres during metaphase-anaphase transition in fission yeast: Dis1 is implicated in force balance in metaphase bipolar spindle. *Mol. Biol. Cell* **9**, 3211-3225.

Nakaseko, Y., Goshima, G., Morishita, J. and Yanagida, M. (2001). M phase-specific kinetochore proteins in fission yeast: microtubule-associating Dis1 and Mtc1 display rapid separation and segregation during anaphase. *Curr. Biol.* **11**, 537-549.

Oliferenko, S. and Balasubramanian, M. K. (2002). Astral microtubules monitor metaphase spindle alignment in fission yeast. *Nat. Cell Biol.* **4**, 816-820.

Pidoux, A. L., Ledizet, M. and Cande, W. Z. (1996). Fission yeast pkl1 is a kinesin-related protein involved in mitotic spindle function. *Mol. Biol. Cell* **7**, 1639-1655.

Pidoux, A. L., Uzawa, S., Perry, P. E., Cande, W. Z. and Allshire, R. C. (2000). Live analysis of lagging chromosomes during anaphase and their effect on spindle elongation rate in fission yeast. *J. Cell Sci.* **113**, 4177-4191.

Popov, A. V., Pozniakovsky, A., Arnal, I., Antony, C., Ashford, A. J., Kinoshita, K., Tournebize, R., Hyman, A. A. and Karsenti, E. (2001). XMAP215 regulates microtubule dynamics through two distinct domains. *EMBO J.* **20**, 397-410.

Rusan, N. M., Fagerstrom, C. J., Yvon, A. M. and Wadsworth, P. (2001). Cell cycle-dependent changes in microtubule dynamics in living cells expressing green fluorescent protein-alpha tubulin. *Mol. Biol. Cell* **12**, 971-980.

Sawin, K. E. and Mitchison, T. J. (1994). Microtubule flux in mitosis is independent of chromosomes, centrosomes, and antiparallel microtubules. *Mol. Biol. Cell* **5**, 217-226.

Tanaka, K. and Kanbe, T. (1986). Mitosis in the fission yeast *Schizosaccharomyces pombe* as revealed by freeze-substitution electron microscopy. *J. Cell Sci.* **80**, 253-268.

Tange, Y., Horio, T., Shimanuki, M., Ding, D.-Q., Hiraoka, Y. and Niwa,

O. (1998). A novel fission yeast gene, tht1+, is required for the fusion of nuclear envelopes during karyogamy. *J. Cell Biol.* **140**, 247-258.

Tirnauer, J. S. and Bierer, B. E. (2000). EB1 proteins regulate microtubule dynamics, cell polarity, and chromosome stability. *J. Cell Biol.* **149**, 761-766.

Tirnauer, J. S., O'Toole, E., Berrueta, L., Bierer, B. E. and Pellman, D. (1999). Yeast Bim1p promotes the G1-specific dynamics of microtubules. *J. Cell Biol.* **145**, 993-1007.

Tran, P. T., Marsh, L., Doye, V., Inoue, S. and Chang, F. (2001). A mechanism for nuclear positioning in fission yeast based on microtubule pushing. *J. Cell Biol.* **153**, 397-411.

Troxell, C. L., Pidoux, A. L., Cande, W. Z. and McIntosh, J. R. (1997). Two nonessential Kar3/Ncd homologues have opposing effects on metaphase spindle length in fission yeast. *Mol. Biol. Cell* **8**, 261A.

Yaffe, M. P., Harata, D., Verde, F., Eddison, M., Toda, T. and Nurse, P. (1996). Microtubules mediate mitochondrial distribution in fission yeast. *Proc. Natl. Acad. Sci. USA* **93**, 11664-11668.